2008 American Control Conference
Westin Seattle Hotel, Seattle, Washington, USA
June 11-13, 2008

Modeling, identification and control of a metrological Atomic Force Microscope with a 3DOF stage

Roel Merry, Mustafa Uyanik, Richard Koops, René van de Molengraft,
Marijn van Veghel and Maarten Steinbuch

Abstract— **Atomic Force Microscopes (AFMs) are widely used for the investigation of samples at nanometer scale. In this paper, we present the modeling, the identification and the control of a metrological AFM. The metrological AFM is used for the calibration of transfer standards for commercial AFMs. Therefore, the focus of the presented work is on scanning accuracy rather than on scanning speed. The contribution of this paper is the combination of 3 degree-of-freedom (DOF) control, including position feedforward, with an AFM with fixed cantilever and a piezo-stack driven stage. The amount of coupling between all DOFs is assessed by a non-parametric MIMO identification of the AFM. Since the dynamics appear to be decoupled in the frequency range of interest, feedback controllers are designed using loopshaping techniques for each DOF separately. Position feedforward is added to the stage in x and y direction, which improves the tracking performance by a factor two. The controlled stage is able to track scanning profiles within the sensor bound of 5 nm. With the proposed control method, the metrological AFM can produce images of the transfer standards with a sensor bound of 2 nm. Furthermore, real-time imaging of the sample is possible without the need for a-posteriori image correction. Finally, it is shown that the proposed control method almost completely compensates the hysteresis in the system.**

I. Introduction

The Atomic Force Microscope (AFM), invented in 1986 by Binning, Quate and Gerber [1], is widely used for sample imaging, the characterization of materials and the manipulation of particles at nanometer scale [2]. AFMs use a probe to 'feel' a surface. The probe has a very sharp tip, which is attached to a cantilever. The sample to be investigated can either be moved under the probe (scanning sample mode) or the probe can be moved over the sample (scanning tip mode). The sample causes the cantilever to deflect. The deflection can be used to obtain the height information of the sample.

In this paper, a metrological AFM is considered. The metrological AFM is used to calibrate transfer standards for commercial AFMs. In contrast to commercial AFMs, the accuracy of the measurements is much more important than the scanning speed. Furthermore, the measurements have to be traceable to the standard of length. This imposes different constraints on both the mechanical and the control design of the AFM.

In present AFMs, the positioning of the sample under the probe, i.e. the scanning motion, is often done using piezoelectric actuators in an open-loop manner [3], [4]. The piezoelectric actuators exhibit nonlinear behavior such as hysteresis and creep, which limit the positioning accuracy of the sample. Furthermore, the mechanical design of the AFM determines the location of the dominant mechanical resonances and with this the achievable bandwidth and the scanning speed. The increasing interest in AFMs for nano-applications requires the need for higher precision and therefore increasing bandwidth.

During the last decades a lot of research on the design, the operating mode and the control of AFMs has been done. The sample manipulation is often performed using tube piezo actuators [5], which can move the sample in three directions using one actuator. The lateral bending of the piezo-tubes results in a cross-coupling into the vertical direction, which distorts the image of the AFM. Tripod scanners employ three piezoelectric stack actuators, one for each translation axis [1]. The path lengths are determined by the length of the stack piezos, resulting in either a small range or low-frequent mechanical resonances and thus low speeds [2]. Resonant scanners use an oscillating tuning fork as actuator to obtain fast scanning [6]. However, the scan rate is dependent on the resonance frequency of the tuning fork and cannot be chosen independently. Stages that stack the actuators for the various degrees-of-freedom (DOFs) typically have a large moving mass, which results in a low-frequent first resonance and in low scanning speed [7]. Piezoelectric stack actuators are combined with a flexure mechanism in rigid scanners [8], [9]. This decouples the different axes of motion to a large extend in combination with a high performance. Therefore, a 3 DOF rigid scanner driven by three piezoelectric stack actuators is used in this paper [10].

Probing of the sample surface can be performed in a static or dynamic manner. In this paper we will only consider static scanning, in which the tip and sample are in contact at all times. The image of the sample is commonly retrieved based on the control effort of the actuator in z-direction. The deflection of the tip can be controlled either in constant force mode, where the force between the sample and the tip is held constant, or in constant height mode, where the feedback is disabled completely [11]. The constant force mode gives high resolution, but only at low speed. The constant height mode allows for faster imaging, but the varying force can damage the sample and/or tip. In this paper, we use constant force scanning in combination with a scanning sample mode to obtain a fully traceable image of the sample.

In literature, the AFMs are mainly identified and modeled

R.J.E. Merry, M. Uyanik, M.J.G. van de Molengraft and M. Steinbuch are with the Eindhoven University of Technology, Department of Mechanical Engineering, Control Systems Technology group, P.O. Box 513, 5600 MB Eindhoven, The Netherlands, r.j.e.merry@tue.nl, http://www.dct.tue.nl

K.R. Koops and M.G.A. van Veghel are with the NMi Van Swinden Laboratorium, Thijsseweg 11, 2629 JA Delft, The Netherlands

978-1-4244-2079-7/08/$25.00 ©2008 AACC.

as three separate SISO systems in x, y (scanning motion) and z (imaging) directions. Furthermore, the MIMO aspects are commonly disregarded without justification [3]. MIMO identification of the scanning motion (x and y directions) only is performed for a tube piezoelectric actuator in [5] and for a 2 DOF nano-positioner driven by piezo-stack actuators in [4]. The coupling to the imaging axis is not taken into account. In this paper, a full MIMO identification in all three directions is performed and the coupling effects between the various axes are explored.

In commercial AFMs, the sample manipulation in x and y directions is commonly performed using only feedforward techniques [3]. Examples of these techniques are H_∞ based [12], [4], [13] and model inverse [14] based feedforward control. However, due to disturbances present in AFMs the performance can benefit from applying feedback control in the scanning directions [2].

In this paper, besides feedback control for the z direction, we also control the x and y directions by means of both feedback and feedforward. This allows the scanning motion to be controlled with a tracking error within the sensor bound of 5 nm.

The contribution of this paper is twofold. Firstly, non-parametric MIMO identification of the AFM in all 3 DOFs is used to investigate the amount of coupling between the various axes and to justify SISO-based controller design. Secondly, feedback control is applied to all 3 DOFs, i.e. also in the scanning direction, of an AFM with fixed cantilever and a piezo-stack driven stage. Loopshaping techniques have been employed to tune three feedback controllers at bandwidths below which the coupling effects can be neglected. Position feedforward is added to the scanning motion, which significantly improves the accuracy. The proposed control method is shown to largely reduce the effect of hysteresis in the system.

This paper is organized as follows. In Section II, the metrological AFM is discussed in more detail. In Section III, MIMO identification is used to retrieve the amount of coupling between the various axes of the AFM. The feedback and feedforward controller design is the subject of Section IV. The results of the experiments are shown in Section V. Finally, conclusions are drawn in Section VI.

II. Metrological AFM

The metrological AFM, shown in Fig. 1, consists of an Topometrix AFM head with optical sensor, a piezo-stack driven 3 DOF stage and a ZYGO interferometer to measure the stage position in all DOFs. The deflection of the cantilever in the AFM head is measured by an optical sensor consisting of a laser and a photodiode. The PI P517.3CL 3 DOF stage [10] is a rigid stage containing three piezo-stack actuators, which can move the stage through a flexure mechanism in a range of 100 μm in x and y directions and in a range of 20 μm in z direction. The resolution and noise bounds of the different sensors are given in Table I.

A schematic representation of the AFM and the feedback control loop is shown in Fig. 2. For clarity the flexure

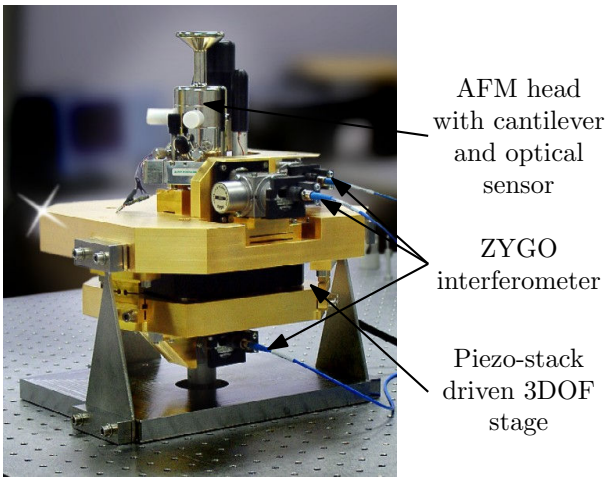

Fig. 1. Picture of the metrological AFM

TABLE I
Resolution and noise bound of the different sensors.

Sensor	Resolution	Noise bound
ZYGO x	0.15 nm	5 nm
ZYGO y	0.15 nm	4 nm
ZYGO z	0.15 nm	2 nm
Head z	0.05 nm	0.15 nm

mechanisms between the piezo-stack actuators and the stage are not shown. Feedback control is applied by steering the piezo-stack actuators while using the ZYGO position measurements in x and y directions. The use of piezo-stack actuators has an advantage over piezo-tube actuators that no direct coupling between the DOFs is present. In z direction, the tip is controlled to a constant deflection while the stage with the sample are moved under the cantilever. Keeping the deflection of the cantilever constant has the advantage that the orientation of the tip compared to the sample topography remains constant. Furthermore, Abbe errors and errors due to the unknown sensitivity of the cantilever are eliminated in this way. Since the tip is controlled to a constant deflection, the laser of the AFM head cannot be used to obtain the sample topography. Instead of using the control effort in z direction, the height of the sample is measured directly using the ZYGO interferometer in z direction. Since the stage position in x and y directions is directly traceable, the image of the sample topography can be constructed using all three ZYGO interferometer measurements.

III. Identification

Although theoretically the different axes are decoupled, practically some amount of cross-coupling can still be present in the 3 DOF stage due to alignment errors. In order to investigate the amount of coupling between the different axes, full non-parametric MIMO identification of the system is performed. The system inputs are the voltages u_i to the piezo-stack actuators and the outputs are the position measurements of the ZYGO interferometer in x,

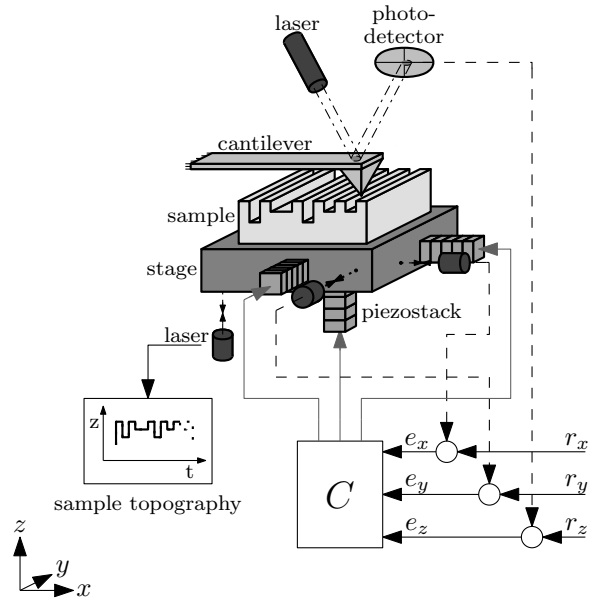

Fig. 2. Schematic representation of the AFM and the feedback control.

and y directions and of the optical sensor in the AFM head in z direction. The MIMO system can be written as

$$P(f) = \begin{bmatrix} P_{XX}(f) & P_{XY}(f) & P_{XZ}(f) \\ P_{YX}(f) & P_{YY}(f) & P_{YZ}(f) \\ P_{ZX}(f) & P_{ZY}(f) & P_{ZZ}(f) \end{bmatrix}, \qquad (1)$$

where $P_{ji}(f)$ denotes the frequency response function (FRF) from the input in i direction to the output in j direction as a function of the frequency f (Hz) and $i \in \{u_x, u_y, u_z\}$, $j \in \{x, y, z\}$.

Using the non-parametric open-loop identification method and Welch's averaged periodogram method [15], the different FRFs in (1) are determined. The bode magnitude plots of the different FRFs in (1) are shown in Fig. 3. The FRFs show a slope of 0 at low frequencies. At frequencies above 40 Hz several resonances can be seen. It can be seen that the amplitude of the off-diagonal FRFs is approximately 40 dB lower than the diagonal FRFs for frequencies $f < 100$ Hz. For frequencies $f \geq 100$ Hz the amplitudes of all FRFs are in the same order of magnitude.

To investigate the amount of coupling between the different axes, the frequency-dependent relative gain array (RGA) of the non-singular square complex matrix $P(f)$ [16], [17] is calculated

$$\text{RGA}(P(f)) = P(f) \times (P(f)^{-1})^T, \qquad (2)$$

where $\times$ denotes element-wise multiplication. The rows and columns of the RGA sum to 1 for all frequencies f. The RGA provides a measure for the amount of interaction. If the $\text{RGA}(f) = I,\ \forall f$, perfect decoupling is achieved. The RGA for the FRFs of Fig. 3 is shown in Fig. 4. It can be seen that for frequencies $f < 100$ Hz, the RGA is almost equal to an identity matrix and therefore for the purpose of feedback controller design the axes may be assumed to be decoupled for frequencies up to 100 Hz. The small amount

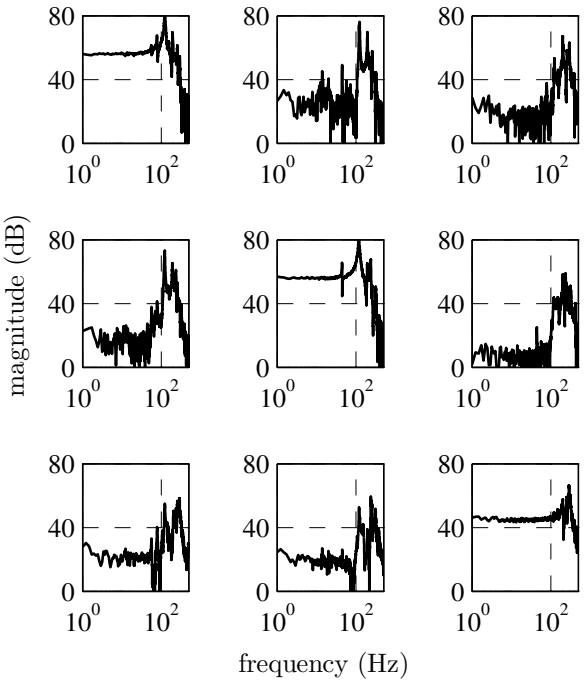

Fig. 3. Bode magnitude plots of the full MIMO system (1)

of coupling for $f < 100$ Hz will still affect the performance of the stage by approximately 1% (40 dB). For frequencies $f \geq 100$ Hz, the RGA shows complete coupling between the different axes.

IV. Controller design

Based on the RGA of Fig. 4, three SISO controllers are designed resulting in bandwidth frequencies $f_{BW} < 100$ Hz, i.e. where no coupling is present. In this paper, we use the definition bandwidth f_{BW} as the cross-over frequency of each loop gain $L(f) = P(f)C(f)$. Moreover, for the x and y axes, position feedforward controllers are designed.

A. Feedback

Using the FRFs of the diagonal elements of (1), feedback controllers C are designed using loopshaping techniques such that the sensitivity

$$|S_{ji}(f)| = \left| \frac{1}{1 + P_{ji}(f)C_{ji}(f)} \right| \leq 6 \text{ dB } \forall f,$$
$$i \in \{u_x, u_y, u_z\},$$
$$j \in \{x, y, z\},$$

corresponding to a phase margin $\phi \geq 30$ deg and an amplitude margin $A \geq 6$ dB. The controllers consist of an integrating action and a low-pass filter as

$$C(s) = k \underbrace{\frac{1}{s}}_{\text{I}} \underbrace{\frac{2\pi f_{LP}}{s + 2\pi f_{LP}}}_{\text{low-pass}}, \qquad (3)$$

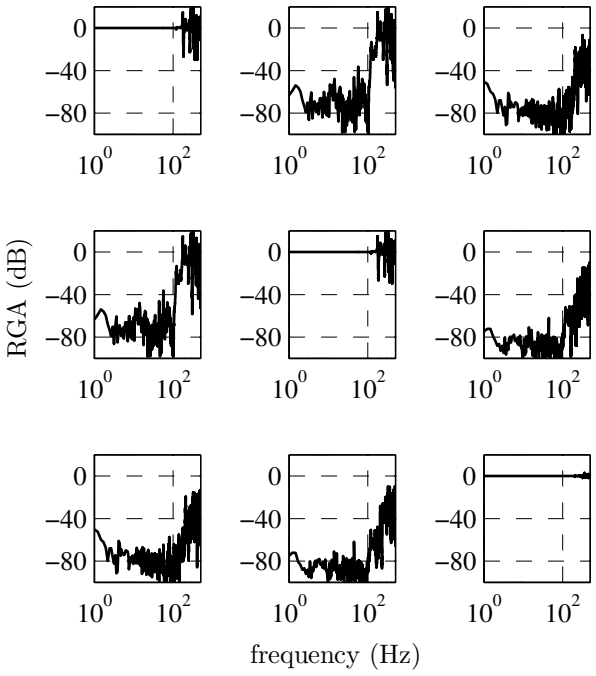

Fig. 4. RGA (2) of the full MIMO system (1)

TABLE II

THE CONTROLLER PARAMETERS, THE RESULTING BANDWIDTH AND THE MODULUS MARGIN FOR THE DIFFERENT AXES.

Axis	k	f_{LP} (Hz)	f_{BW} (Hz)	$\|S\|_\infty$ (dB)
x	0.07790	50	7.87	3.635
y	0.07790	50	8.03	4.052
z	0.1198	100	45.6	4.939

where k denotes the controller gain and f_{LP} the frequency where the integrating action ends. In Table II, the controller designs, the resulting bandwidths f_{BW} and the modulus margin $\|S\|_\infty$ for the different axes are shown. The margins are chosen somewhat higher to be robust against shifts in the resonance frequencies due to the nonlinearities in the piezo-stack actuators [4].

The characteristic loci $\lambda(PC)$ [16] are shown in the left part of Fig. 5. The characteristic loci show the controlled MIMO system has a good MIMO phase margin. The Nyquist plots of the separate diagonal loop gains, depicted in the right part of Fig. 5, almost coincide with the characteristic loci, i.e. $\lambda(PC) \approx \lambda(diag(PC))$. This again indicates that the different axes are almost decoupled. Furthermore, the diagonal loop gains are stable and do not enter the circle with radius 0.5 centered at (Re,Im)=(-1,0), indicating that $|S(f)| < 6$ dB $\forall f$.

B. Feedforward

Stability of the closed loop system is guaranteed by the feedback controllers. The performance can be largely improved by accounting for the known setpoint trajectories for x and y, which act as a known disturbance on the closed-loop system. A position feedforward is added since the piezo-stack actuators act as a position actuator. The control input of the feedforward is added to the output of the feedback controllers $u_i,\ i \in \{x, y\}$, resulting in a new input to the system u^* as

$$u_i^*(t) = u_i(t) + Kr_i(t), \quad i \in \{x, y\},$$

where K denotes the feedforward gain and r the reference signal. For the z axis, position feedforward is not useful since the reference position for the z-axis is a constant. The sample topography is unknown and not assumed to be equal for adjacent scans. Therefore, also this information cannot be used for feedforward control in the z direction.

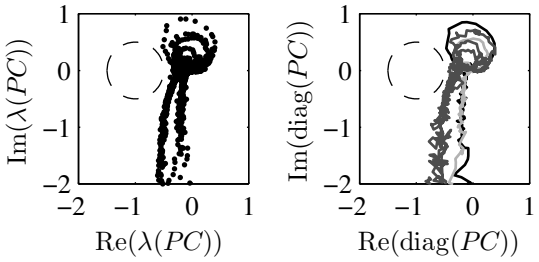

Fig. 5. Characteristic loci $\lambda(P(f)C(f))$ (left part) and Nyquist plots of the separate diagonal loop gains (right part) in x direction (black), y direction (dark grey) and z direction (light grey).

V. RESULTS

In this section, the results of the experiments on the metrological AFM of Fig. 1 are discussed. Scanning experiments are performed in x direction. The y direction is controlled to a constant position.

A. Scanning motion

In Fig. 6, the measured positions of the stage both with and without feedforward are shown for a scan over 40 μm with a speed of 2 $\mu m/s$. For the x and y axes, the feedforward gains are chosen as $K_x = K_y = 11$. The tracking errors show an improvement in the scanning accuracy due to the feedforward of a factor two. The largest errors are obtained at the turning points of the triangular shaped reference signal. These errors can be reduced by smoothing of the reference signal at the turn-around points.

The cumulative power spectral densities (PSDs) of the tracking errors are shown in the right part of Fig. 6. For frequencies $f \to \infty$, the cumulative PSDs converge with and without feedforward to 23.84 nm^2 and 821.9 nm^2 respectively, which are equal to the squared root-mean-square (rms) values of the respective errors.

The sample topography, measured by the ZYGO interferometer in z direction, is shown as a function of the position in x direction in Fig. 7. Since a triangular shaped reference is used in x direction, the topography of Fig. 7 contains the measured height of the sample for a scan in both positive and negative x direction. No large deviations of the height can

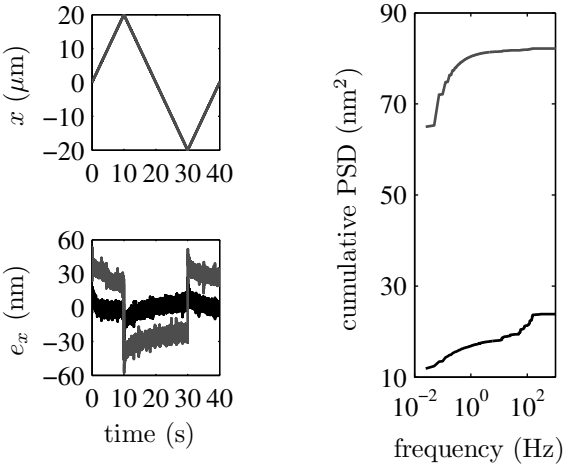

Fig. 6. Measured positions, tracking errors and cumulative PSDs of the tracking errors in x direction, reference (dashed), with (black) and without (dark-grey, PSD/10) feedforward.

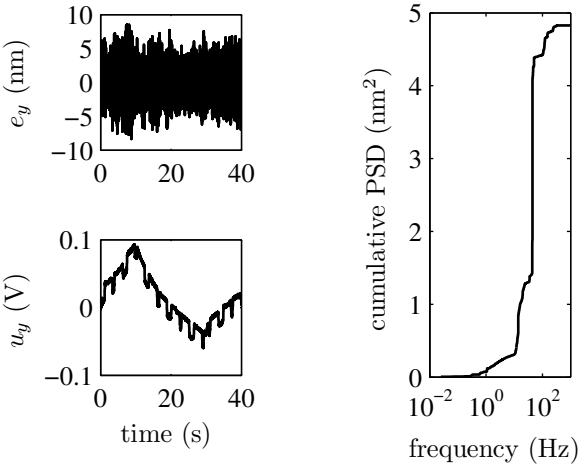

Fig. 8. Tracking error (left top), control effort (left bottom) and cumulative PSD (right) in y direction.

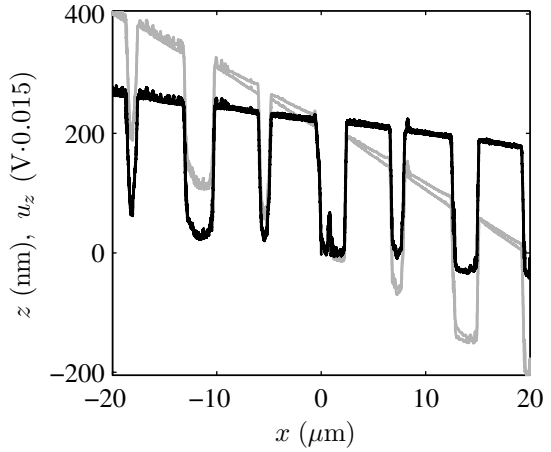

Fig. 7. Measured topography of the sample with the ZYGO interferometer (black) and constructed topography using the control effort in z direction (grey).

be seen. The measured topography shows a decaying height in x direction, indicating that the sample is tilted under the AFM.

Since the output of the ZYGO interferometer is used instead of the control effort in z direction, as is done in most literature, the height of the sample is directly measurable and traceable. The reconstructed topography using the control effort in z direction is shown in Fig. 7 by the grey line. The reconstructed topography clearly shows a global slope difference between the measured height of the ZYGO laser and the reconstructed height. This difference is likely to be caused by misalignments between the piezo-stack actuator and the ZYGO interferometer in z direction and by the fact that the piezo-stack actuator is not calibrated. Furthermore, a clear distinction can be made between the reconstructed height in positive and negative x direction as two lines are visible. The control effort in z direction also contains influences of the hysteresis and creep of the piezo-stack actuators and of the small amount of coupling between the different DOFs. This causes the errors in the constructed topography. Further postprocessing of the data in combination with a good knowledge of the system characteristics is required to better reconstruct the sample topography from the control effort in z direction.

During the experiment, the y axis is controlled to a fixed position. The tracking error in y direction is shown in Fig. 8 together with the control effort. The shape of the control effort clearly shows a correlation with the sample topography of Fig. 7. Based on the FRF of the system (see Fig. 3) a coupling of 1% between the axes was expected for frequencies $f < 100$ Hz. The cumulative PSD, shown in the right of Fig. 8, converges for $f \to \infty$ to 4.83 nm^2.

B. Hysteresis

The piezo-stack actuators exhibit hysteresis. The hysteresis measured in the system in x direction for a scan over 40 μm with a speed of 2 μm/s is shown in Fig. 9 by the left part. The feedback loop clearly reduces the amount of hysteresis present in the system as can be seen in the right part of Fig. 9. However, still some small amount of hysteresis remains, as shown in the detailed plot in the right part of Fig. 9.

C. Scanning speed

The tracking errors are dependent on the scanning speed. Real-time imaging of the sample is only possible if the scanning movement is controlled within the sensor noise bound during the imaging periods, i.e. except for the turning points where no image is made. The maximum absolute values and the rms values of the tracking errors for various

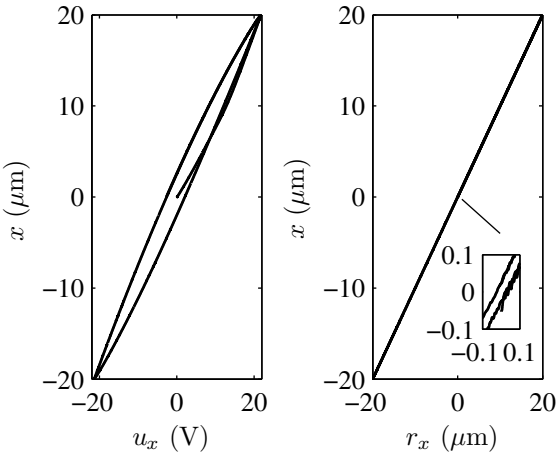

Fig. 9. Hysteresis plot of the system (left) and with feedback (right).

TABLE III
MAXIMUM ABSOLUTE TRACKING ERRORS FOR VARYING REFERENCE SPEEDS.

Speed	$\max(\lvert e_x(t)\rvert)$ (nm)	$\text{rms}(\lvert e_x(t)\rvert)$ (nm)
1 μm/s	18.16	3.05
2 μm/s	29.11	4.88
4 μm/s	47.67	9.02
8 μm/s	88.95	17.77

scans speeds are shown in Table III. The error increases with increasing scanning speed.

In order to increase the scanning speed, the tracking errors have to be reduced. One possible solution is the increase of the bandwidth of the system. However, this would require MIMO control since decoupling of the axes is no longer guaranteed when increasing the bandwidth f_{BW} much further (see Fig. 4).

VI. CONCLUSIONS

In this paper, the modeling, the identification and the control of a metrological AFM are presented. For calibration purposes the measurements have to be fully traceable, which imposes different design considerations on the microscope and the control.

The contribution of this paper is the combination of three degree-of-freedom (DOF) control on a AFM with fixed cantilever and a piezo-stack driven stage.

Using a full non-parametric MIMO model of the system, the coupling between the different axes has been investigated using the frequency dependent relative gain array (RGA). The RGA shows that for the purpose of feedback controller design the axes can be considered to be decoupled up to a frequency of 100 Hz.

The feedback controllers are designed using loopshaping techniques. Position feedforward control in x and y directions improve the scanning performance by a factor two. Furthermore, the effect of hysteresis in the piezo driven stage has been reduced significantly by the feedback control loop.

With the presented control method, the AFM can perform scanning movements with a velocity of 2 μm/s and a tracking error within the sensor bound of 5 nm. A separate laser is used to measure the sample topography directly through the stage movement in vertical direction. Images of the sample are obtained with a sensor bound of 2 nm.

With the presented feedback loop, still a small amount of hysteresis is present in the feedback controlled system. This could be compensated for using a hysteresis feedforward.

Although the system is almost decoupled for frequencies $f < 100$ Hz, still a small amount of coupling is present, which can be accounted for using MIMO control methods.

REFERENCES

[1] G. Binning, C. F. Quate, and C. Gerber, "Atomic force microscope," *Physical Review Letters*, vol. 56, no. 9, pp. 930–933, 1986.

[2] G. Schitter, "Advanced mechanical design and control methods for atomic force microscopy in real-time," *American Control Conference*, pp. 3503–3508, 2007.

[3] L. Y. Pao, A. Butterworth, and D. Y. Abramovich, "Combined feedforward/feedback control of atomic force microscopes," *American Control Conference*, pp. 3509–3515, 2007.

[4] A. Sebastian and S. M. Salapaka, "Design methodologies for robust nano-positioning," *IEEE Transactions on Control Systems Technology*, vol. 13, no. 6, pp. 868–876, 2005, 1063-6536.

[5] A. Daniele, S. Salapaka, M. V. Salapaka, and M. Dahleh, "Piezoelectric scanners for atomic force microscopes: design of lateral sensors, identification and control," *American Control Conference*, vol. 1, pp. 253–257, 1999.

[6] A. Humphris, M. Miles, and J. Hobbs, "A mechanical microscope: High-speed atomic force microscopy," *Applied physics letters*, vol. 86, no. 3, p. 034106, 2005.

[7] T. Ando, N. Kodera, E. Takai, D. Maruyama, *et al.*, "A high-speed atomic force microscope for studying biological macromolecules," *Proceedings of the National Academy of Sciences*, vol. 98, no. 22, pp. 12 468–12 472, October 2001.

[8] J. H. Kindt, G. E. Fantner, J. A. Cutroni, and P. K. Hansma, "Rigid design of fast scanning probe microscopes using finite element analysis," *Ultramicroscopy*, vol. 100, no. 3-4, pp. 259–265, 2004.

[9] G. Schitter, G. E. Fanter, P. J. Thurner, J. Adams, *et al.*, "Design and characterization of a novel scanner for high-speed atomic force microscopy," *IFAC Mechatronics conf.*, pp. 819–824, 2006.

[10] *P-517, P-527 Multi-Axis, Piezo Nanopositioning / Scanning Stages with Parallel Metrology*, PI, 2005, www.physikinstrumente.com.

[11] G. Schitter, P. Menold, H. F. Knapp, F. Allgöwer, *et al.*, "High performance feedback for fast scanning atomic force microscopes," *Review of Scientific Instruments*, vol. 72, no. 8, pp. 3320–3327, 2001.

[12] A. Stemmer, G. Schitter, J. M. Rieber, and F. Allgöwer, "Control strategies towards faster quantative imaging in atomic force microscopy," *European Journal of Control*, vol. 11, no. 4-5, pp. 384–395, 2005.

[13] S. Salapaka, A. Sebastian, J. P. Cleveland, and M. V. Salapaka, "Design, identification and control of a fast nanopositioning device," *American Control Conference*, vol. 3, pp. 1966–1971, 2002.

[14] Q. Zou and S. Devasia, "Preview-based optimal inversion for output tracking: application to scanning tunneling microscopy," *IEEE Transactions on Control Systems Technology*, vol. 12, no. 3, pp. 375–386, 2004, 1063-6536.

[15] L. Ljung, *System Identification: theory for the user*, 2nd ed. Prentice Hall, 1999, ISBN 0-13-656695-2.

[16] S. Skogestad and I. Postlethwaite, *Multivariable Feedback Control, analysis and design*, 2nd ed. John Wiley & Sons, 2005, ISBN 0-470-01168-8.

[17] E. Bristol, "On a new measure of interaction for multivariable process control," *IEEE Transactions on Automatic Control*, vol. 11, no. 1, pp. 133–134, 1966, 0018-9286.